Inorganic Chemistry

pubs.acs.org/IC Article

Self-Assembled Lanthanide Phosphinate Square Grids (Ln = Er, Dy, and Tb): Dy_4 Shows SMM/SMT and Tb_4 SMT Behavior

Suman Mondal, Deepanshu Chauhan, Thierry Guizouarn, Fabrice Pointillart,* Gopalan Rajaraman,* Alexander Steiner,* and Viswanathan Baskar*

Cite This: *Inorg. Chem.* 2024, 63, 22338−22348

Read Online

ACCESS | Metrics & More | Article Recommendations | Supporting Information

ABSTRACT: Tetranuclear [2 × 2] square-grid-like Ln^{III} clusters have been synthesized by reacting $LnCl_3 \cdot 6H_2O$ salts with bis[α-hydroxy(p-bromophenyl)methyl]phosphinic acid [R_2PO_2H, where R = CH(OH)PhBr] and pivalic acid. Single-crystal X-ray diffraction studies show the formation of $[\mathrm{Me_4N}]_2[\mathrm{Ln_4}(\mu_2\text{-}\eta^1{:}\eta^1\text{-}\mathrm{PO_2R_2})_8(\eta^2\text{-}\mathrm{CO_2Bu^t})_4(\mu_4\text{-}\mathrm{CO_3})]$ [Ln = Er (**1**), Dy (**2**), and Tb (**3**)]. Direct-current studies reveal significant ferromagnetic interactions between Dy^{III} in **2** and Tb^{III} in **3** and an antiferromagnetic interaction between Er^{III} in **1**. Dynamic magnetic susceptibility measurements confirm a single-molecule magnet (SMM) behavior in both 0 and 1200 Oe applied magnetic fields for **2**. Complexes **2** and **3** show single molecular toroic (SMT) behavior with a mixed magnetic moment.

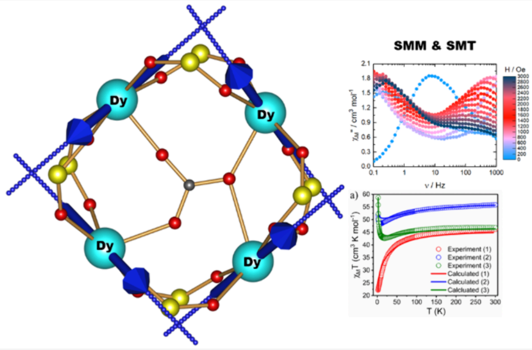

■ INTRODUCTION

Polynuclear lanthanide clusters have attracted great attention in the past decades due to their applications in various fields like luminescence,[1,2] catalysis,[3] magnetic refrigeration,[4−8] and molecule magnets[9] such as single-ion magnets (SIMs), single-chain magnets (SCMs), single-molecule magnets (SMMs). Among them, molecular magnetism has been investigated extensively since the discovery of the famous Mn_{12}-acetate SMM behavior.[10] Lanthanide ions that have inherent large single-ion anisotropy and magnetic bistability are key components for the assembly of novel SMMs. U_{eff} (anisotropic energy barrier) and T_B (blocking temperature) are the two terms associated with SMM behavior. Large U_{eff} and high T_B values are required for potential applications. Dy, Tb, and Er are the most promising candidates for SMM due to their large spin−orbit coupling and high magnetic moments.[9] Very recently, two Dy compounds have been reported that show a high blocking temperature (20 K)[11] and an effective energy barrier (1025 K).[12] Dy SMMs are the most interesting among the lanthanides due to their strong uniaxial magnetic anisotropy ($g_z \gg g_{x,y}$). Dinuclear,[13] trinuclear,[14] tetranuclear (butterfly, square, cubane, rhombus shape, chainlike, linear, Y-shape, see-saw, and zigzag irregular shape),[15−51] and higher-nuclear[52−54] lanthanide clusters are reported in the literature.

Among them, tetranuclear Dy clusters have shown interesting SMM behavior, as reported by Chandrasekhar et al.[55] Tong et al. have observed that the tetranuclear [2 × 2] grid topology showed the highest U_{eff} (143 cm^{-1}).[56] Self-assembled polymetallic square [$n \times n$] (n = 2−5) (M_4−M_{25}) complexes are quite common for transition metals such as Mn, Fe, Co, Ni, Cu, and Zn with poly-n-topic hydrazone-based ligands.[57−59] The first genuine heteroleptic self-assembled [2 × 2] grid was reported by Murugesu et al.[60] The grid arrangement of Dy shows a high U_{eff} (270 K) (τ_0 = 4.0 × 10^{-10} s); its peak maxima shifted toward the high-temperature regime, which implies a reduction of quantum tunnelling of magnetization (QTM). Several square grids [2 × 2] were synthesized utilizing thiolate, thiacalix[4]arene, triazole, Schiff base, hydrazide, and hydrazone-based Schiff base ligands.[30,56,60−78]

Polynuclear complexes, which are bistable molecules with a toroidal magnetic state, are defined as single-molecule toroics (SMTs).[79,80] SMTs are characterized by the vortex arrangement of magnetic dipoles,[81−83] $T = \sum_{j=1}^{N} r_i s_i$ ($N \geq 2$ spins per unit cell; T = toroidal magnetic moment, r = displacement of the magnetic ions from the center position, s = spins of the magnetic ions). The [Dy_3] triangle, reported by Powell's group in 2006, first demonstrated the fascinating properties of SMM even though it has a nonmagnetic ground state[14] furnishing a new class of magnetic materials.[82,83] Tong et al. in 2012 first reported the tetranuclear toroidal moment SMT for planar Dy_4 clusters.[84] This area of research is a growing field; the property

Received: June 20, 2024
Revised: August 26, 2024
Accepted: September 3, 2024
Published: September 12, 2024

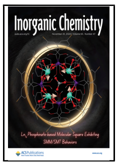

of SMT is not limited to the planar [Dy_3] triangle,[14,54,85−92] but several wheel shape topologies, viz., [Dy_4] planar,[84] [Dy_4] square,[68,73,75] [Dy_6] wheel,[93−98] and coupled [Dy_3],[91] have been prepared since. Recently, [Dy_4] cubic and [Dy_4] tetrahedral topologies have been reported, expanding the area from planar (2D) to nonplanar (3D) SMTs.[99]

Several factors influence a molecule's SMT behavior, including its wheel-shaped topology, the arrangement of magnetic anisotropic axes in a circular/planar manner, high molecular site symmetry, oblate−prolate electron densities of Ln ions, and dipolar coupling.[100] While planarity helps to enhance the toroidicity, Le Guennic and co-workers recently developed 3D SMTs lacking any planarity for Ln^{III} ions.[99] Moreover, the lanthanide ion's magnetic exchange interaction and dipolar coupling should be strong and favorable to stabilize the toroidal ground state.[101] Experimentally, it has been noted that the S-shape magnetization indicates SMT behavior. Still, in isolation, this signal cannot be taken as an indication for a toroidal moment because a diamagnetic ground state with a closely lying excited paramagnetic state and no toroidal behavior can also show an S-shape curve.[102]

Herein we have synthesized a series of isostructural lanthanide complexes (**1**−**3**) of [2 × 2] grid topology using the bis[α-hydroxy(p-bromophenyl)methyl]phosphinate ligand and pivalate as the coligand. To our knowledge, this is the first example of a square-grid [2 × 2] complex that is assembled by using a phosphinate ligand.

RESULTS AND DISCUSSION

Synthesis. The ligand was synthesized according to the literature procedure.[103,104] Complexes **1**−**3** were synthesized as summarized in Scheme 1. The hydrated lanthanide chloride salts were added to a methanolic solution of the ligand, followed by the base tetramethylammonium hydroxide in a 1:2:2 ratio. A clear solution was obtained when stirred for 30 min at room temperature. A mixture of pivalic acid and tetramethylammonium hydroxide (1:1) was added. After 5 h, volatiles were removed and the white solid was washed twice with diethyl ether and kept for crystallization in acetonitrile. Single-crystal X-ray-quality crystals were obtained after slow evaporation of the solution. The products were characterized by standard analytical and spectroscopic techniques.

Scheme 1. Synthesis of [2 × 2] Tetranuclear Ln_4 Complexes 1−3

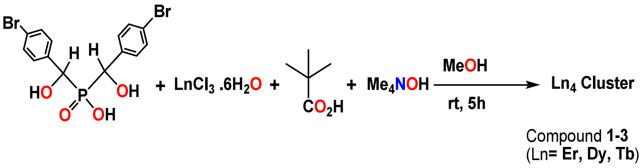

The IR spectra of **1**−**3** (Figures S1, S9, and S17) show the characteristic peaks of aromatic and aliphatic C−H stretching of the ligand of around 2868−2970 cm^{-1}, O−H stretching of the ligand between 3344 and 3359 cm^{-1}, water bending at 1645−1646 cm^{-1}, P−O stretching of around 1008−1069 cm^{-1}, C−O stretching (for CH_2OH) at 1169−1192 cm^{-1}, symmetric CO_3^-/CO_2^- stretching at 1364−1369 cm^{-1}, asymmetric CO_3^-/CO_2^- stretching at around 1524−1534 cm^{-1}, aromatic C−Br stretching at 1103 cm^{-1}, C═C stretching at 1435−1484 cm^{-1}, and C−H out-of-plane bending at around 821−822 cm^{-1}.

Thermogravimetric analysis (TGA) studies (Figures S2, S10, and S18) reveal that major weight loss occurred for **1**−**3** at 289, 287, and 288 °C, respectively. This loss corresponds to ligand dissociation and trapped solvent. The crystallinity and phase purity of the bulk samples for **1**−**3** were verified by the powder X-ray diffraction (PXRD) data (Figures S8, S16, and S24).

Crystal Structures. Compounds **1**−**3** are isostructural, crystallizing in tetragonal space group $I422$ with $Z = 4$. The two independent anionic complexes occupy sites of symmetry 422. Their charge is balanced by tetramethylammonium cations that occupy the void spaces between them. The dianionic complexes contain four Ln^{III} centers that are arranged in a planar square 2 × 2 grid. They are bridged by eight phosphinate ligands, four of which are located above and four below the plane of the Ln_4 square. In addition, there are four pivalate ions, each chelating a Ln center in a bidentate fashion. Finally, there is a carbonate ion at the center of the complex, which is disordered because it is incompatible with crystallographic site symmetry 422. The presence of the disordered carbonate ion breaks the crystallographic symmetry of the complex, resulting in the chemical inequivalence of the four Ln centers (Figure 1a). The two independent anionic complexes are enantiomers but otherwise very much identical. They are distinguished by their relative orientation to the cell axes: The edges of the Ln_4 square of one enantiomer are aligned parallel, while those of the other enantiomer are diagonal to the lattice direction ⟨100⟩.

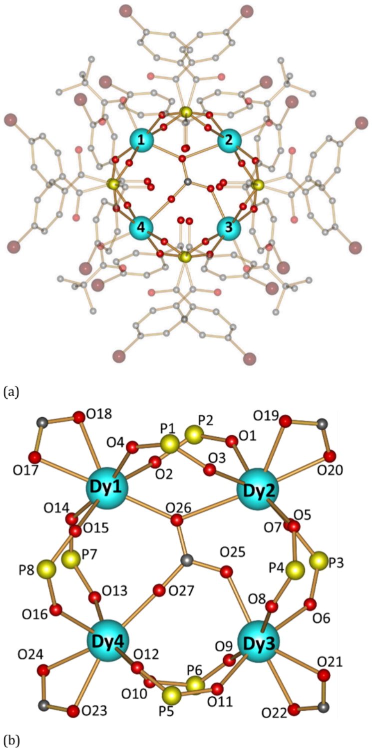

Figure 1. (a) Ball-and-stick views of the molecular structure of **2**. (b) Ball-and-stick view of the core structure of **2**. Hydrogen atoms are omitted for clarity. Key: red, O; gray, C; yellow, P; brown, Br; cyan, Dy.

The Ln centers are heptacoordinated; their coordination environment can be described as distorted pentagonal-bipyramidal (see the SHAPE analysis in Table S2). They bind to four oxygen atoms of four phosphinate ligands, two oxygen atoms of the bidentate pivalate ligands, and one oxygen atom of the centrally located carbonate ion (Figure 1b). In the core structure, two neighboring Ln centers are connected via two phosphinate ligands in a [2.11] mode based on the Harris notation, while each Ln center coordinates to one bidentate pivalate ligand in a [1.11] mode. The carbonate ion connects in a [4.112] mode to the four Ln centers. The distances between Ln centers along the edge of the square range between 4.66 and 4.70 Å, while the distances diagonally across the square range from 6.59 to 6.65 Å. The shortest intermolecular Ln···Ln distances are just above 12 Å. The Ln−O bond distances fall in the expected ranges (Table 1). Selected bond distances and angles are given in Tables S3−S5.

Table 1. Important Bond Distances (Å) for Complexes 1−3 in This Work[a]

Er···Er	Dy···Dy	Tb···Tb
4.657	4.676	4.701
Er···Er^d	Dy···Dy^d	Tb···Tb^d
6.586	6.613	6.648
Er−O$_{PA}$	Dy−O$_{PA}$	Tb−O$_{PA}$
2.252−2.255	2.242−2.277	2.245−2.316
Er−O$_{piv}$	Dy−O$_{piv}$	Tb−O$_{piv}$
2.428	2.442	2.462
Er−O$_{CO_3}$	Dy−O$_{CO_3}$	Tb−O$_{CO_3}$
2.117−2.775	2.151−2.685	2.207−2.653
Er···Er^{ps}	Dy···Dy^{ps}	Tb···Tb^{ps}
12.094	12.048	12.117

[a] d = diagonal, PA = phosphinic acid, piv = pivalic acid, and ps = packing shortest.

In addition to metal coordination, the complexes are held together by intramolecular hydrogen bonding, which involves the hydroxy groups of the phosphinate ligands. Each ligand has two such groups, one interacting with the hydroxy group of another phosphinate ligand (resulting in eight hydrogen bonds, four below and four above the central plane), while the other is bonding to oxygen atoms of the pivalate ligands (yielding another eight hydrogen bonds; Figure S11c). In addition, the two phenyl rings of each phosphinate ligand form a $\pi-\pi$ interaction (Figure S14b,c).

It should be noted that carbonate compounds were not used as precursors in the syntheses of compounds 1−3. However, it is well-documented that lanthanide salts, when contained in a basic medium, can attract atmospheric CO$_2$, resulting in the incorporation of carbonate ions.[105] In this case, the carbonate ion also acts as a template in the formation of the square-grid core structure.

Magnetic Properties. Direct-current (dc) magnetic susceptibility measurements were performed on immobilized polycrystalline powder samples of **1**−**3** (Figure 2). The observed room temperature $\chi_M T$ values of 46.15 cm^{-3} K mol^{-1} for **1**, 55.84 cm^{-3} K mol^{-1} for **2**, and 46.83 cm^{-3} K mol^{-1} for **3** are in agreement with four Er^{III} ($^4I_{15/2}$, $g_J = {}^6/_5$, and $\chi_M T = 45.92$ cm^{-3} K mol^{-1}), Dy^{III} ($^6H_{15/2}$, $g_J = 4/3$, and $\chi_M T =$ 56.68 cm^{-3} K mol^{-1}), and Tb^{III} ($^7F_6$, $g_J = {}^3/_2$, and $\chi_M T = 47.28$ cm^{-3} K mol^{-1}), respectively.[106] Upon cooling, the $\chi_M T$ values were found to be almost constant down to 100 K, and below this temperature, the $\chi_M T$ product started decreasing for all of the compounds. For **1**, $\chi_M T$ reaches a minimum value of 22.15 cm^{-3} K mol^{-1} at 2 K, while the $\chi_M T(T)$ curves increase below 10 and 15 K to reach values of 51.82 and 58.71 cm^{-3} K mol^{-1} at 2 K for **2** and **3**, respectively. The decrease of the $\chi_M T$ value can be mainly attributed to the thermal depopulation of the m_J levels, while the low temperature increase would be due to ferromagnetic interactions between the Ln^{III} ions. The field-dependent magnetization measurements were performed on complexes **1**−**3** at 2 K (Figure S25). The magnetization reaches the values of 19.24, 20.60, and 18.62 Nβ at 50 kOe without saturation for **1**−**3**, respectively. The observed lower magnetization values suggest the presence of magnetic anisotropy in these systems due to strong spin−orbit coupling resulting from an unquenched orbital angular momentum.

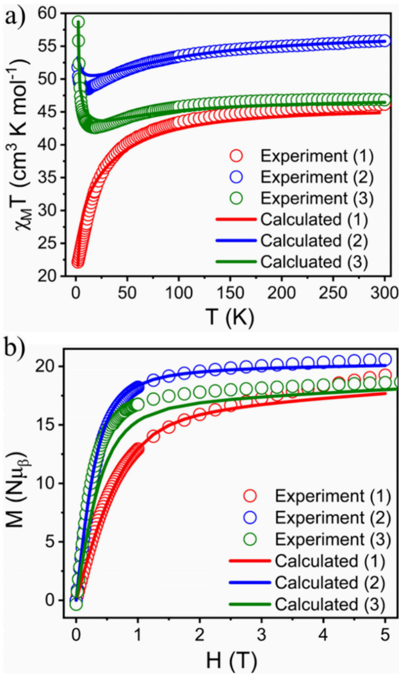

Figure 2. Temperature-dependent $\chi_M T$ versus T plot for complexes **1**−**3**. The solid lines are the fitted data from *POLY_ANISO*.

The slow magnetic relaxation behavior of **1**−**3** was investigated by performing frequency-dependent alternating-current (ac) magnetic susceptibility measurements. In zero applied dc field ($H = 0$ Oe), only the tetranuclear complex **2** displayed slow magnetic relaxation (Figure S26) with an out-of-phase component (χ_M'') maximum centered at 8 Hz at 2 K (Figure 3a). **1** and **3** did not show any slow magnetic relaxation at 0 Oe (Figures S27 and S28). Under zero applied dc field, **2** displays a frequency dependence of the magnetic susceptibility in the temperature range 2−15 K (Figures S29 and 3b). The relaxation time (τ) has been extracted with an extended Debye model (eq S1 and Table S6).[107,108] The normalized Argand plot demonstrated that, at 2 K, 50% of the sample is involved in the slow magnetic relaxation (Figure S30). In other words, only one of the two crystallographically independent Dy^{III} molecules presents a slow magnetic relaxation in the 1−1000 Hz frequency range.

The corresponding thermal variation of log(τ) is plotted in Figure 3d for the temperature range of 2−15 K. The log[$\tau(T)$] curve was fitted using eq 1:

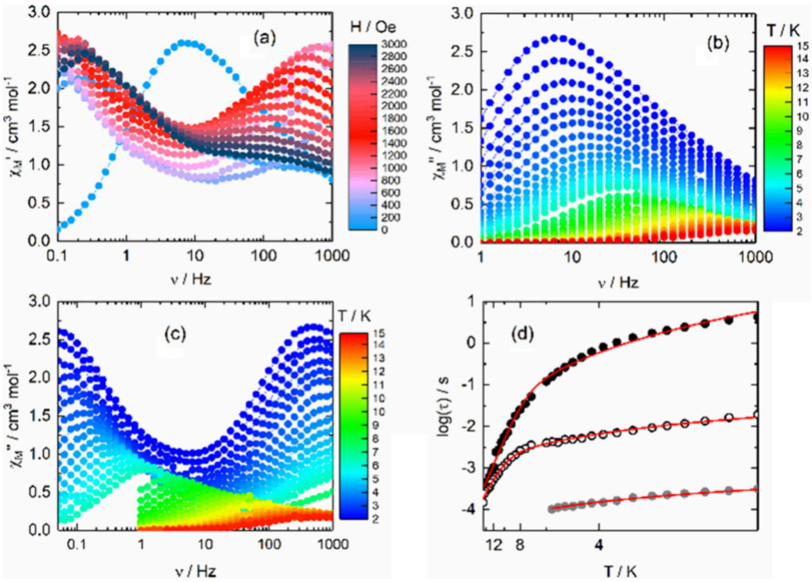

Figure 3. (a) Field dependence of the ac χ_M'' magnetic susceptibility for **2** at 2 K in the 0−3000 Oe field range. (b) Frequency dependence of χ_M'' in the 2−15 K temperature range under zero applied dc field. (c) Frequency dependence of χ_M'' in the 2−15 K temperature range under the applied dc field of 1.2 kOe. (d) Thermal dependence of log(τ) for **2** under zero applied dc field (open black circles) and under 1200 Oe applied field for the LF (full black dots) and HF (full gray dots) contributions. Full red lines are the best-fitted curves with parameters given in the text.

$$\tau^{-1}(T, H) = AH^4T + \frac{B_1}{1 + B_2H^2} + \underbrace{\tau_0^{-1}e^{U_{\mathrm{eff}}/k_BT} + CT^n}_{k(T)} \quad (1)$$

where the four terms correspond respectively from left to right to the direct, QTM, Orbach and Raman processes. The best-fitted curve is represented in Figure 3d with a combination of Orbach [$\Delta = 80(4)$ K and $\tau_0 = 1.03(3) \times 10^{-6}$ s] and Raman [$C = 23.8(17)$ s^{-1} K^{-n} and $n = 1.33(5)$] processes (Figure S31). The n exponent is very weak compared to the theoretical one for a Kramer lanthanide ion ($n = 9$), indicating a strong involvement of acoustic phonons (lattice vibrations) in the Raman relaxation mechanism.[109−112] In zero applied dc field, one could expect a QTM contribution; nevertheless, the addition of such a process does not improve the fit. The relatively weak QTM contribution might be attributed to the significant ferromagnetic interaction between the Dy^{III} ions. The fast relaxation of 50% of Dy^{III} could be imputed to QTM. It is well-known that such a process can be efficiently suppressed by applying an external dc field. The field dependence of the magnetic susceptibility was investigated for the **1−3** compounds. Under an applied magnetic field, compounds **1** and **3** displayed a χ_M'' contribution with maxima localized at frequencies higher than 10 kHz (Figures S27 and S28). For **2**, the χ_M'' contribution is shifted to lower frequency (LF) under an applied magnetic field (0.05 Hz at 2 K for H = 1200 Oe), and a second χ_M'' contribution appeared at higher frequency (HF; 400 Hz at 2 K for H = 1200 Oe). The frequency of the magnetic susceptibility under an applied magnetic field of 1200 Oe was depicted in Figures 3c and S32. The normalized Argand plot under 1200 Oe applied field is in agreement with a slow magnetic relaxation part representing more than 80% of the sample (Figure S33). Thus, the fast magnetic relaxation through QTM for the one of the two Dy^{III} ions is canceled by applying a dc field. The relaxation times were extracted by simultaneously fitting χ_M' and χ_M'' using an extended Debye model (Table S7) accounting for two single relaxation contributions using eq S2 for $T < 7$ K, while a single relaxation was taken into account for $T \geq 7$ K (eq S1). The corresponding thermal variation of log(τ) is plotted in Figure 3d. The best-fitted curves were obtained using a direct process only [$A = 7.88(8) \times 10^{-10}$ s^{-1} K^{-1} Oe^{-m} with $m = 4$ (fixed)] for the HF contribution (Figure S34) and a combination of Orbach [$\Delta = 87(4)$ K and $\tau_0 = 9.39(3) \times 10^{-7}$ s] and Raman ($C = 1.78(3) \times 10^{-2}$ s^{-1} K^{-n} and $n = 3.28(13)$] processes for the LF contribution (Figure S35). The energy barrier of the Dy$_4$ square-grid complex of this paper is compared with the so-far-obtained Dy$_4$ square grid in the literature review, which exhibits SMM behavior at zero applied dc field (Table S18).

Theoretical Section. Magnetic Exchange Interactions. We employed BS-DFT calculations to compute the isotropic magnetic exchange interactions, replacing the Dy^{III} ion with a Gd^{III} ion and rescaling the computed parameters for other Ln^{III} ions, as is well-established in the literature.[101] We extracted two coupling parameters: one for the neighbor nearest to the Ln ion (J_1) and another for the neighbor diagonal to the Ln ion [J_2; see computational details in the Supporting Information (SI) for more information].

Ab Initio Calculations. To investigate the mechanism of magnetic relaxation, the nature of magnetic anisotropy, and, more importantly, the toroidal behavior in these complexes of **1−3**, ab initio calculations were performed (Table 2). Here, we performed CASSCF/RASSI-SO/SINGLE_ANISO calculations on the X-ray structure, with the peripheral ligand geometry simplified to reduce the computational time (see computational details in the SI). The bridging carbonate molecules are highly disordered. To check the effect of carbonate disorder, we performed calculations on complex **2** considering both carbonate bridging positions. Because both models yielded the same results, we conducted the calculations for complexes **1** and **3** similarly on one model. The distance between the Ln ion and the O ion of the carbonate bridge ranges between 2.157 and 2.663 Å for **1**, between 2.229 and 2.690 Å for **2**, and between 2.223 and 2.667 Å for complex **3**. This variation in the distance results in subtle differences in the crystal field and single-ion anisotropy for each ion. To account

Table 2. Summary of the Results of Complexes 1 and 3 from Ab Initio Calculations

complex	SMM	SMT, type	T_z	M/μ_B
1	no	no		
2	yes	yes, mixed moment	≠0	16.42
3	no	yes, mixed moment	≠0	11.94
Main Values of the Ground-State **g** Tensors				
	Er1	Er2	Er3	Er4
g_x	0.025	0.131	0.119	0.115
g_y	0.071	0.616	0.521	0.626
g_z	16.464	16.436	16.342	16.419
	Dy1	Dy2	Dy3	Dy4
g_x	0.007	0.007	0.010	0.041
g_y	0.013	0.009	0.017	0.082
g_z	19.770	19.849	19.772	19.711
	Tb1	Tb2	Tb3	Tb4
g_x	0.000	0.000	0.000	0.000
g_y	0.000	0.000	0.000	0.000
g_z	17.032	17.155	17.213	17.384

for this, we have computed the single-ion anisotropic parameters for each ion, which, despite being crystallographically symmetric, are influenced by the disorder of the carbonate. The computational model, therefore, includes all four Ln ions. This variation impacts the crystal-field splitting for each ion, which we have examined in detail by analyzing **g** tensors and crystal-field parameters. The magnetic exchange/dipolar coupling between Ln^{III} ions was estimated by fitting the experimental magnetic data using the Lines model with the *POLY_ANISO* program.[113] The following Hamiltonian was used to extract the exchange parameters:

$$\hat{H}_{\mathrm{ex}} = -\sum_{i=1}^{2} J_i \cdot S_i \cdot S_{i+1}$$

Here $J_i = J_i^{\mathrm{dipolar}} + J_i^{\mathrm{exchange}}$; i.e., J_i values are the total magnetic interactions in the combination of calculated J_i^{dipolar} and fitted J_i^{exchange} parameters; this describes the interaction between the intramolecular metal centers.

Mechanism of Magnetization Relaxation of Single Ln^{III} Centers. To begin, we performed calculations on single-ion Er^{III}/Dy^{III}/Tb^{III} complexes (**1**−**3**) by substituting the other Ln^{III} ions with diamagnetic elements to understand the magnetic behavior of the complex under extreme dilution conditions. To begin with, all four Dy^{III} centers in complex **2** were found to be asymmetric with the ground−first excited state gaps of 217.1, 228.2, 209.1, and 199.2 cm^{-1} for Dy1, Dy2, Dy3, and Dy4, respectively. For prolate complex **1**, the gaps were estimated to be 41.3, 89.2, 109.7, and 77.2 cm^{-1} for Er1−4, respectively. While the gaps are similar, differences are attributed to the difference in the Dy/Er−O bond lengths and the corresponding bond angles. This is also reflected in the computed g anisotropies, with all four exhibiting Ising anisotropies g_{zz} = 19.770, 19.849, 19.772, and 19.711 for Dy1−4 and g_{zz} = 14.464, 16.436, 16.342, and 16.419 with varying degrees of transverse component for Er1−4 in complex **2** (Table S11). For complex **2**, the corresponding g_{zz} axis aligns in the molecular plane (Figures 4 and S40). The ground-state QTM was found to be small for Dy2, and it was found to be the largest for Dy4, reflecting the transverse anisotropy trend computed. Therefore, the relaxation was expected via the first Kramers doublets, as exemplified by the corresponding noncoincidence of the g_{zz} axis and the higher TA-QTM values. This suggests that the single-ion barrier height is the same as that of the gap mentioned above, with four different barrier heights ranging from 199 to 228 cm^{-1}, suggesting multiple relaxation pathways at lower temperatures. This is also supported by the computed crystal-field parameters, which indicate the presence of a larger nonaxial component (in which $q \neq 0$ and $k = 2$, 4, and 6) rather than an axial component (in which $q = 0$ and $k = 2$, 4, and 6), supporting prominent QTM effects (Table S9). However, the experimental value obtained from the magnetic studies is much larger, suggesting that single-ion relaxation is not the key mechanism observed. For complex **1**, the transverse anisotropy is significant, as is also reflected in the computed QTM at the ground state, suggesting relaxation via the ground state. The g_{zz} axis for complex **1** is directed toward the middle of the ring and found not to form any circular arrangement in complex **2**. This is also supported by the estimated crystal-field parameters (Table S12). Due to its non-Kramer's nature, complex **3** differs from complexes **1** and **2**. Here as well, the first excited state is found to be different among Tb1−4 with gaps of 77.5, 85.6, 84.1, and 127.6, respectively, with the g_{zz} value varying in the range of 17.032−17.384, with an extremely large tunnel splitting for Tb1, Tb3, and Tb4 with a relatively smaller one for Tb2 (Table S14). In all cases, the ground state is dominantly $m_J = \pm 6$, with the g_{zz} axis direction resembling that of complex **3**. Because strong axiality is lacking, coupled with strong equatorial ligation, the tunnel splitting observed suggests the absence of any SMM characteristics for this complex, as witnessed in the experiments.

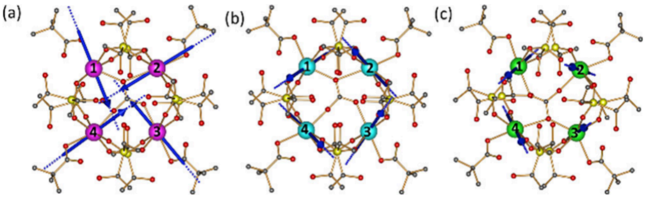

Figure 4. Orientation of the magnetic anisotropic axis. (a) Direction of the ground-state magnetic anisotropic axis in complex **1**. (b) Direction of the ground-state magnetic anisotropic axis in complex **2**. (c) Direction of the ground-state magnetic anisotropic axis in complex **3**.

Relaxation Mechanism, Including Exchange Coupling and SMT Behavior. Because the single-ion relaxation mechanism failed to rationalize the experimental observation, we constructed the relaxation mechanism for the tetrameric unit using the *POLY_ANISO* program, where the experimental susceptibility and magnetization data were simulated using the Lines model to obtain the magnetic exchange and the dipolar coupling constants (Table 3).[114] The magnetic susceptibility data gave good fitting with the parameters $J_1 = 0.2$, $J_2 = -0.1$, and $zJ = 0.0$ for complex **2** (similarly for **1** and **3**; Table 3). So, the magnetic exchange calculation suggests ferromagnetic dipolar coupling in complexes **2** and **3** and antiferromagnetic dipolar coupling in **1**, which has also been noted in other reports.[115] Despite the asymmetry of all four Ln^{III} ions, we used a single J value to avoid overparameterization concerns. This approach allows us to streamline our analysis, ensuring a more straightforward interpretation of magnetic interactions while accounting for the complexity of the individual ions. Overall, two exchanges are considered: J_1 for nearest-neighbor exchange and J_2 for next-nearest neighbor exchange consider-

Table 3. Computed Exchange and Dipolar Couplings (cm^{-1}) of Complexes 1−3

	J_1			J_2			
complex	J_{exch}	J_{dip}	J_{tot}	J_{exch}	J_{dip}	J_{tot}	z_J
1	0.005	−0.995	−1.0	−0.009	−0.791	−0.8	0.0
2	0.008	0.192	0.2	−0.015	−0.085	−0.1	0.0
3	0.010	0.690	0.7	−0.018	−0.102	−0.12	0.0

ing a very short $Ln^{III}\cdots Ln^{III}$ distance and the proximity of the ligands. The best-fit yield antiferromagnetic exchange (J_{exch}) for complex **1** and ferromagnetic exchange for complexes **2** and **3** with J_1 are estimated to be stronger than J_2 interactions. Further, complexes **2** and **3** exhibit relatively stronger exchanges than complex **1**. The J_{dip} exchange, on the other hand, was found to be ferromagnetic for complexes **2** and **3** but was found to be antiferromagnetic for complex **1**. Because J_{dip} was found to be dominant over J_{exch} in all cases, the sign of the overall exchange is dictated by the dipolar coupling contribution with the overall ferromagnetic J in the case of complexes **2** and **3** and antiferromagnetic J for **1**. It is worth noting that the main contribution to the magnetic coupling in carbonate bridge complexes **1**−**3** arises from the magnetic dipolar coupling rather than from the exchange coupling. The dipolar contribution to the magnetic exchange coupling can be calculated by the following equation:

$$J_{dip} = -\left\{\frac{\mu_0}{4\pi}\right\}\frac{\mu_i\mu_j}{r^3}[3\cos^2(\theta) - 1]$$

where μ_i and μ_j represent the magnetic moments of centers i and j, respectively, μ_0 denotes the vacuum permittivity, r is the distance between them, and θ is the angle between the orientation of the magnetic moments and the vector connecting the two interacting centers.[116] This expression results in antiferromagnetic coupling for $\theta > 54.75°$ and ferromagnetic coupling for $\theta < 54.75°$.[117] Moreover, this equation implies an antiferromagnetic coupling for an angle between the magnetic moments and the molecular plane (θ) greater than 66.2° and a ferromagnetic coupling for angles lower than this threshold (specifically, for an angle of 60.8° between the magnetic moments i and j, the threshold angle value for a colinear system is 54.7°).[118] The magnitude of θ reflects the strength of the antiferromagnetic dipolar coupling; the larger the angle, the stronger the exchange parameter.[119] The estimated J_{dip} values from the above equation, with the Hamiltonian $H_{dip} = -J_{dip}J_1J_2$ (where J_1J_2 represents the m_J values of the doublet ground state of the i and j centers) for complexes **1**−**3**, are shown in Table 3.

The mechanisms constructed for complexes **1** and **2** are shown in Figures S44 and 5, respectively. Due to stronger dipolar interaction and the g_{zz} orientation of the Dy^{III}/Tb^{III} lying on the plane perpendicular to the pseudo-C_4 axis, both complexes were found to exhibit a mixed toroidal moment exemplified by the computed total moment at the ground state (using $\mu_z = {}^1/_2 g_z\mu_B$) with values of 16.42 μ_B for **1** and 11.94 μ_B for **3** with a nonzero T_z value.[120] The toroidal states are found to disperse within 2.3 cm^{-1}, beyond which spin-flip states were found at 199.2 cm^{-1} for complex **2**. While this value is also more significant than the experimental value, because exchange coupling is relatively weak (less than 1 cm^{-1}), single-ion relaxation at elevated temperatures cannot be ruled out. Similarly, complex **3** was also found to have mixed toroidal moments with the spin-flip states stabilized at 2 cm^{-1} and hence does not offer a magnetization blockade like that seen in complex **2**.

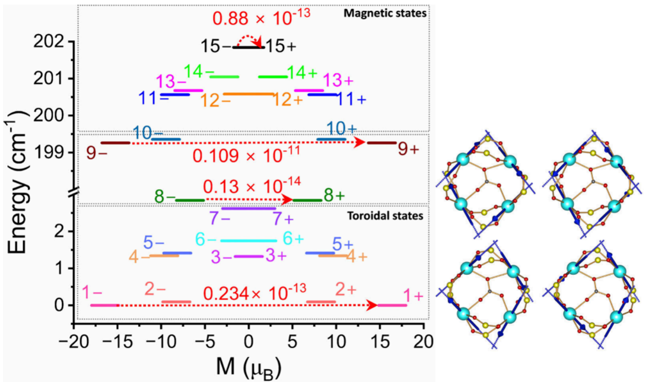

Figure 5. Low-lying magnetic exchange spectrum of complex **2**. The exchange magnetic states are placed on the diagram according to their magnetic moment value (bold lines). The dashed red arrow shows the QTM within each doublet. Near Kramer doublets, the pictures indicate the direction of the magnetic moment in toroidal or vortex arrangements.

■ CONCLUSIONS

We have successively synthesized and characterized a tetranuclear self-assembled Ln_4 square [2 × 2] grid-like topology where the four Ln centers lie in the same plane. This is the first example of such an assembly that uses phosphinate ligands. The central carbonate ion originates from atmospheric carbon dioxide, which acts as a template in the formation of the square-grid core structure. Magnetic investigations demonstrated that significant ferromagnetic interactions occurred between the lanthanide centers [except for Er^{III}(antiferromagnetic)] and SMM behavior is present in both zero and applied magnetic fields for **2**, with magnetic relaxation occurring through multiple processes. Compounds **2** and **3** show a mixed toroidal magnetic moment.

■ EXPERIMENTAL SECTION

Instrumentation. IR spectra were recorded with a Nicolet iS5 FTIR spectrometer. Elemental analysis was performed with a Flash EA Series 1112 CHNS analyzer. TGA was recorded with a PerkinElmer STA 8000 thermogravimetric analyzer under a nitrogen gas flow rate of 20 mL/min and a heating rate of 10 °C/min. The single-crystal X-ray diffraction (SCXRD) data for **1**−**3** were collected at 100 K with a Bruker APEX-II CCD diffractometer system [λ(Mo Kα) = 0.71073 Å] with a graphite monochromator using the $\varphi-\omega$ scan technique. The data were reduced using the Bruker *SAINT* package. Absorption correction was performed using the *SADABS* program. The structures were solved by direct methods and refined on F^2 by full-matrix least squares using the program *SHELXL-2018/3*. The structure was solved with *OLEX2*[121] and the *ShelXT*[122] structure solution program using intrinsic phasing and refined with the *SHELXL 2018/3*[123,124] refinement package using least-squares minimization. All non-hydrogen atoms were refined anisotropically, and hydrogen atoms were fixed at calculated positions and refined as a horse riding model. EADP, RIGU, SIMU, DELU, SADI, and FLAT constrained/restrained commands were used to fix the disordered atoms. Graphics of the crystal structures were done with the *Diamond* (version 2.1e) and *Mercury* (version 3.10.3) software. The details of the data are given in the SI. For **2**, the *OLEX2* solvent mask (similar to *PLATON/SQUEEZE*) was used to mask out the electron density of the disordered molecules. The details of the solvent masks used are given below.

For compound **2**, a solvent mask was calculated and 36 electrons were found in a volume of 1720 Å^3 in 1 void. This is consistent with the presence of 4 H_2O molecules per formula unit, which accounts for 160.0 electrons.

The dc magnetic susceptibility measurements were performed on an immobilized solid polycrystalline sample with a Quantum Design MPMS-XL SQUID magnetometer between 2 and 300 K in an applied magnetic field of 0.02 T for temperatures of 2−20 K, 0.2 T for temperatures of 20−80 K, and 1 T for temperatures of 80−300 K. The ac magnetic susceptibility measurements were performed on a Quantum Design MPMS-XL SQUID for frequencies between 0.1 and 1000 Hz and a Quantum Design PPMS magnetometer for frequencies between 100 and 10000 Hz. These measurements were all corrected for the diamagnetic contribution, as calculated with Pascal's constants.

General Information. All of the general reagents were purchased commercially and used without further purification. Bis[α-hydroxy(*p*-bromophenyl)methyl]phosphinic acid [R_2PO_2H, where R = CH(OH)PhBr] was prepared by the reported procedure.[103,104] Hydrated lanthanide chloride salts were prepared from their corresponding oxides by neutralization with concentrated HCl, followed by evaporation to dryness.

The synthetic procedure followed for the synthesis of these complexes is detailed below.

Synthesis. To a 60 mL methanolic solution of R_2PO_2H [R = CH(OH)PhBr] was added $LnCl_3{\cdot}6H_2O$, and the resulting solution was stirred for a few minutes (2−3 min). Then dropwise tetramethylammonium hydroxide was added, and stirring was continued. After 30 min, a 2 mL methanolic solution of pivalic acid with Me_4NOH was added to it. The reaction mixture was stirred for 5 h at room temperature. The solvent was evaporated with rotary vapor. A white solid was formed, washed with diethyl ether twice, and crystallized in acetonitrile to get X-ray-quality single crystals.

Compound **1**. R_2PO_2H (0.100 g, 0.229 mmol), $ErCl_3{\cdot}6H_2O$ (0.043 g, 0.114 mmol), pivalic acid (0.023 g, 0.229 mmol), Me_4NOH (in 25% MeOH; 0.035 mL + 0.011 mL, 0.458 mmol). Yield: 0.92 g, 70.76% (based on $ErCl_3{\cdot}6H_2O$). Anal. Calcd for $Br_{16}C_{141}Er_4H_{156}N_2O_{43}P_8$ (4762.03): C, 35.56; H, 3.30; N, 0.59. Found: C, 35.62; H, 3.35; N, 0.63. IR (cm^{-1}): 3352.37 (br), 2962.16 (m), 2872.02 (w), 1645.27 (w), 1534.57 (s), 1484.33 (s), 1435.83 (w), 1403.47 (s), 1362.17 (m), 1171.52 (s), 1069.73 (s), 1008.60 (s), 948.74 (s), 906.91 (m), 863.42 (m), 821.87 (s), 703.87 (w), 605.00 (w), 557.40 (m).

Compound **2**. R_2PO_2H (0.100 g, 0.229 mmol), $DyCl_3{\cdot}6H_2O$ (0.042 g, 0.114 mmol), pivalic acid (0.023 g, 0.229 mmol), Me_4NOH (in 25% MeOH; 0.035 mL + 0.011 mL, 0.458 mmol). Yield: 0.085 g, 66.40% (based on $DyCl_3{\cdot}6H_2O$). Anal. Calcd for $Br_{16}C_{141}Dy_4H_{158}N_2O_{44}P_8$ (4761.00): C, 35.57; H, 3.35; N, 0.59. Found: C, 35.93; H, 3.44; N, 0.63. IR (cm^{-1}): 3344.72 (br), 2970.18 (m), 2872.02 (w), 1645.54 (w), 1575.64 (w), 1524.34 (s), 1484.89 (s), 1436.30 (m), 1401.19 (m), 1364.32 (w), 1192.49 (m), 1169.89 (s), 1103.55 (w), 1069.20 (s), 1008.88 (s), 947.75 (m), 907.36 (m), 863.97 (m), 821.57 (s), 776.38 (w), 730.28 (m), 704.21 (w), 648.11 (w), 607.37 (w), 555.58 (m).

Compound **3**. R_2PO_2H (0.100 g, 0.229 mmol), $TbCl_3{\cdot}6H_2O$ (0.042 g, 0.114 mmol), pivalic acid (0.023 g, 0.229 mmol), Me_4NOH (in 25% MeOH; 0.035 mL + 0.011 mL, 0.458 mmol). Yield: 0.089 g, 68.99% (based on $TbCl_3{\cdot}6H_2O$). Anal. Calcd for $Br_{16}C_{141}Tb_4H_{156}N_2O_{43}P_8$ (4728.67): C, 35.81; H, 3.33; N, 0.59. Found: C, 35.83; H, 3.60; N, 0.71. IR (cm^{-1}): 3359.15 (br), 2961.85 (m), 2868.84 (w), 1646.07 (w), 1530.96 (s), 1484.22 (s), 1439.01 (w), 1401.73 (s), 1369.11 (w), 1192.49 (m), 1169.92 (s), 1103.60 (w), 1068.98 (s), 1008.53 (s), 948.28 (s), 905.04 (m), 862.64 (m), 822.42 (s), 774.93 (w), 729.77 (m), 703.69 (m), 647.98 (w), 605.09 (w), 556.37 (m).

■ ASSOCIATED CONTENT

Supporting Information

The Supporting Information is available free of charge at https://pubs.acs.org/doi/10.1021/acs.inorgchem.4c02567.

> Crystallographic data, selected bond metric parameters, ORTEP diagrams for all compounds, IR, TGA, PXRD, SHAPE calculations, SEM images, ab initio calculation of the magnetism, and ac susceptibility data (PDF)

Accession Codes

CCDC 2294080−2294082 contain the supplementary crystallographic data for this paper. These data can be obtained free of charge via www.ccdc.cam.ac.uk/data_request/cif, or by emailing data_request@ccdc.cam.ac.uk, or by contacting The Cambridge Crystallographic Data Centre, 12 Union Road, Cambridge CB2 1EZ, UK; fax: +44 1223 336033.

■ AUTHOR INFORMATION

Corresponding Authors

Fabrice Pointillart − *Sciences Chimiques de Rennes, Universite de Rennes 1, UMR 6226, CNRS 263, Rennes 35042, France;* orcid.org/0000-0001-7601-1927; Email: fabrice.pointillart@univ-rennes1.fr

Gopalan Rajaraman − *Department of Chemistry, Indian Institute of Technology Bombay, Powai, Mumbai 400076, India;* orcid.org/0000-0001-6133-3026; Email: rajaraman@chem.iitb.ac.in

Alexander Steiner − *Department of Chemistry, University of Liverpool, Liverpool L69 7ZD, U.K.;* orcid.org/0000-0002-4315-6123; Email: a.steiner@liverpool.ac.uk

Viswanathan Baskar − *School of Chemistry, University of Hyderabad, Hyderabad 500046, India;* orcid.org/0000-0002-5270-3272; Phone: +91-40-23134825; Email: vbsc@uohyd.ac.in

Authors

Suman Mondal − *School of Chemistry, University of Hyderabad, Hyderabad 500046, India;* orcid.org/0000-0003-4892-7350

Deepanshu Chauhan − *Department of Chemistry, Indian Institute of Technology Bombay, Powai, Mumbai 400076, India*

Thierry Guizouarn − *Sciences Chimiques de Rennes, Universite de Rennes 1, UMR 6226, CNRS 263, Rennes 35042, France*

Complete contact information is available at: https://pubs.acs.org/10.1021/acs.inorgchem.4c02567

Author Contributions

The concept of the work was designed by V.B. Synthesis and characterization of the molecules and optimization of the protocol were done by S.M. Magnetic data collection and data analysis were done by T.G. and F.P. The computational studies and explanation of the theoretical data of the SMM/SMT behavior were done by D.C. and G.R. A.S. helped in refinement of the SCXRD data. S.M. and D.C. wrote the initial draft of the manuscript, and V.B., G.R., F.P., and A.S. added corrections.

Notes

The authors declare no competing financial interest.

■ ACKNOWLEDGMENTS

V.B. thanks SERB for funding (CRG/2023/000684). S.M. thanks the UGC for a fellowship.

■ REFERENCES

(1) Shi, Y.; He, L.; Wang, X.; Wu, Z.; Gao, N.; Zhang, H.; Wang, W.; Cui, J. A novel terbium metal−organic framework for luminescence sensing of pyridine: Synthesis, structure, selectivity, sensitivity and recyclability. *J. Rare Earths* **2020**, *38*, 1231−1236.

(2) Heine, J.; Müller-Buschbaum, K. Engineering metal-based luminescence in coordination polymers and metal−organic frameworks. *Chem. Soc. Rev.* **2013**, *42*, 9232−9242.

(3) Wu, Z.; Lan, X.; Zhang, Y.; Li, M.; Bai, G. Copper(I) iodide cluster-based lanthanide organic frameworks: synthesis and application as efficient catalysts for carboxylative cyclization of propargyl alcohols with CO_2 under mild conditions. *Dalton Trans.* **2019**, *48*, 11063−11069.

(4) Das, C.; Upadhyay, A.; Ansari, K. U.; Ogiwara, N.; Kitao, T.; Horike, S.; Shanmugam, M. Lanthanide-based porous coordination polymers: syntheses, slow relaxation of magnetization, and magnetocaloric effect. *Inorg. Chem.* **2018**, *57*, 6584−6598.

(5) Liu, S. J.; Cao, C.; Xie, C. C.; Zheng, T. F.; Tong, X. L.; Liao, J. S.; Chen, J. L.; Wen, H. R.; Chang, Z.; Bu, X. H. Tricarboxylate-based Gd^{III} coordination polymers exhibiting large magnetocaloric effects. *Dalton Trans.* **2016**, *45*, 9209−9215.

(6) Liu, S. J.; Han, S. D.; Zhao, J. P.; Xu, J.; Bu, X. H. In-situ synthesis of molecular magnetorefrigerant materials. *Coord. Chem. Rev.* **2019**, *394*, 39−52.

(7) Zheng, T. F.; Tian, X. M.; Wu, L. H.; Liu, S. J.; Yao, S. L.; He, K. H.; Huang, H.; Liao, J.; Chen, J. L.; Wen, H. R. Two Gd III complexes with different structures and magnetocaloric properties induced by metal ion sources. *New J. Chem.* **2019**, *43*, 18445−18450.

(8) Liu, S. J.; Cao, C.; Yao, S. L.; Zheng, T. F.; Wang, Z. X.; Liu, C.; Liao, J. S.; Chen, J. L.; Li, Y. W.; Wen, H. R. Temperature-and vapor-induced reversible single-crystal-to-single-crystal transformations of three 2D/3D Gd(III)−organic frameworks exhibiting significant magnetocaloric effects. *Dalton Trans.* **2017**, *46*, 64−70.

(9) Woodruff, D. N.; Winpenny, R. E.; Layfield, R. A. Lanthanide single-molecule magnets. *Chem. Rev.* **2013**, *113*, 5110−5148.

(10) Sessoli, R.; Gatteschi, D.; Caneschi, A.; Novak, M. A. Magnetic bistability in a metal-ion cluster. *Nature* **1993**, *365*, 141−143.

(11) Chen, Y. C.; Liu, J. L.; Ungur, L.; Liu, J.; Li, Q. W.; Wang, L. F.; Ni, Z. P.; Chibotaru, L. F.; Chen, X. M.; Tong, M. L. Symmetry-supported magnetic blocking at 20 K in pentagonal bipyramidal Dy (III) single-ion magnets. *J. Am. Chem. Soc.* **2016**, *138*, 2829−2837.

(12) Liu, J.; Chen, Y. C.; Liu, J. L.; Vieru, V.; Ungur, L.; Jia, J. H.; Chibotaru, L. F.; Lan, Y.; Wernsdorfer, W.; Gao, S.; Chen, X. M.; Tong, M. L. A stable pentagonal bipyramidal Dy (III) single-ion magnet with a record magnetization reversal barrier over 1000 K. *J. Am. Chem. Soc.* **2016**, *138*, 5441−5450.

(13) Long, J.; Habib, F.; Lin, P. H.; Korobkov, I.; Enright, G.; Ungur, L.; Wernsdorfer, W.; Chibotaru, L. F.; Murugesu, M. Single-molecule magnet behavior for an antiferromagnetically superexchange-coupled dinuclear dysprosium (III) complex. *J. Am. Chem. Soc.* **2011**, *133*, 5319−5328.

(14) Tang, J.; Hewitt, I.; Madhu, N. T.; Chastanet, G.; Wernsdorfer, W.; Anson, C. E.; Benelli, C.; Sessoli, R.; Powell, A. K. Dysprosium triangles showing single-molecule magnet behavior of thermally excited spin states. *Angew. Chem.* **2006**, *118*, 1761−1765.

(15) Jami, A. K.; Ali, J.; Mondal, S.; Homs-Esquius, J.; Sañudo, E. C.; Baskar, V. Dy_2 and Dy_4 hydroxo clusters assembled using o-vanillin based Schiff bases as ligands and β-diketone co-ligands: Dy_4 cluster exhibits slow magnetic relaxation. *Polyhedron* **2018**, *151*, 90−99.

(16) Liu, C. M.; Hao, X. Asymmetric assembly of chiral lanthanide (III) tetranuclear cluster complexes using achiral mixed ligands: Single-molecule magnet behavior and magnetic entropy change. *ACS omega* **2022**, *7*, 20229−20236.

(17) Gebrezgiabher, M.; Schlittenhardt, S.; Rajnák, C.; Sergawie, A.; Ruben, M.; Thomas, M.; Boča, R. A Tetranuclear Dysprosium Schiff Base Complex Showing Slow Relaxation of Magnetization. *Inorganics* **2022**, *10*, 66.

(18) Kumar, P.; Swain, A.; Acharya, J.; Li, Y.; Kumar, V.; Rajaraman, G.; Colacio, E.; Chandrasekhar, V. Synthesis, structure, and zero-field SMM behavior of homometallic Dy_2, Dy_4, and Dy_6 complexes. *Inorg. Chem.* **2022**, *61*, 11600−11621.

(19) Yang, C.; Wei, Y. H.; Xu, S.; Zhang, H. Y.; Yang, Y. Q.; Zhang, B.; Fang, M. Single molecule magnet behavior and magnetic refrigeration of carbonyl oxygen-bridged tetranuclear lanthanide complexes. *New J. Chem.* **2021**, *45*, 14103−14110.

(20) Grebenyuk, D.; Zobel, M.; Polentarutti, M.; Ungur, L.; Kendin, M.; Zakharov, K.; Degtyarenko, P.; Vasiliev, A.; Tsymbarenko, D. A Family of Lanthanide Hydroxo Carboxylates with 1D Polymeric Topology and Ln_4 Butterfly Core Exhibits Switchable Supramolecular Arrangement. *Inorg. Chem.* **2021**, *60*, 8049−8061.

(21) Zhang, Y. X.; Zhang, Y. H.; Liu, B. Y.; Wang, W. M.; Tang, G. P.; Wei, H. Y.; Wu, Z. L. Synthesis, luminescence and magnetic properties of tetranuclear lanthanide-based (Eu_4, Gd_4 and Dy_4) clusters. *New J. Chem.* **2018**, *42*, 18305−18311.

(22) Zhu, Z. H.; Wang, H. F.; Yu, S.; Zou, H. H.; Wang, H. L.; Yin, B.; Liang, F. P. Substitution effects regulate the formation of butterfly-shaped tetranuclear Dy(III) cluster and Dy-based hydrogen-bonded helix frameworks: structure and magnetic properties. *Inorg. Chem.* **2020**, *59*, 11640−11650.

(23) Shi, Y.; Zhang, Y. X.; Li, M.; Zhang, Y. H.; Liu, B. Y.; Tang, G. P.; Zhang, Z. Q.; Liu, K. X.; Wu, Z. L.; Wang, W. M. Two novel tetranuclear lanthanide complexes (Ln= Tb (III) and Dy (III)) with luminescence and slow magnetic relaxation behaviors. *Polyhedron* **2019**, *157*, 292−296.

(24) Gao, H. L.; Huang, S. X.; Zhou, X. P.; Liu, Z.; Cui, J. Z. Magnetic properties and structure of tetranuclear lanthanide complexes based on 8-hydroxylquinoline Schiff base derivative and β-diketone coligand. *Dalton Trans.* **2018**, *47*, 3503−3511.

(25) Zhang, Y. X.; Li, M.; Liu, B. Y.; Wu, Z. L.; Wei, H. Y.; Wang, W. M. A series of planar tetranuclear lanthanide complexes: axial ligand modulated magnetic dynamics in Dy_4 species. *RSC Adv.* **2017**, *7*, 55523−55535.

(26) Langley, S. K.; Chilton, N. F.; Gass, I. A.; Moubaraki, B.; Murray, K. S. Planar tetranuclear lanthanide clusters with the Dy_4 analogue displaying slow magnetic relaxation. *Dalton Trans.* **2011**, *40*, 12656−12659.

(27) Biswas, S.; Das, S.; Gupta, T.; Singh, S. K.; Pissas, M.; Rajaraman, G.; Chandrasekhar, V. Observation of Slow Relaxation and Single-Molecule Toroidal Behavior in a Family of Butterfly-Shaped Ln_4 Complexes. *Chem. Eur. J.* **2016**, *22*, 18532−18550.

(28) Gao, H. L.; Jiang, L.; Liu, S.; Shen, H. Y.; Wang, W. M.; Cui, J. Z. Multiple magnetic relaxation processes, magnetocaloric effect and fluorescence properties of rhombus-shaped tetranuclear rare earth complexes. *Dalton Trans.* **2016**, *45*, 253−264.

(29) Alexandropoulos, D. I.; Cunha-Silva, L.; Pham, L.; Bekiari, V.; Christou, G.; Stamatatos, T. C Tetranuclear lanthanide (III) complexes with a zigzag topology from the use of pyridine-2, 6-dimethanol: synthetic, structural, spectroscopic, magnetic and photoluminescence studies. *Inorg. Chem.* **2014**, *53*, 3220−3229.

(30) Yadav, M.; Mondal, A.; Mereacre, V.; Jana, S. K.; Powell, A. K.; Roesky, P. W. Tetranuclear and pentanuclear compounds of the rare-earth metals: synthesis and magnetism. *Inorg. Chem.* **2015**, *54*, 7846−7856.

(31) Lin, S. Y.; Tang, J. Versatile tetranuclear dysprosium single-molecule magnets. *Polyhedron* **2014**, *83*, 185−196.

(32) Liu, C. M.; Zhang, D. Q.; Zhu, D. B. A single-molecule magnet featuring a parallelogram $[Dy_4\ (OCH_2^{\ -})_4]$ core and two magnetic relaxation processes. *Dalton Trans.* **2013**, *42*, 14813−14818.

(33) Rasamsetty, A.; Das, C.; Sañudo, E. C.; Shanmugam, M.; Baskar, V. Effect of coordination geometry on the magnetic properties of a series of Ln_2 and Ln_4 hydroxo clusters. *Dalton Trans.* **2018**, *47*, 1726−1738.

(34) Lin, S. Y.; Zhao, L.; Ke, H.; Guo, Y. N.; Tang, J.; Guo, Y.; Dou, J. Steric hindrances create a discrete linear Dy_4 complex exhibiting SMM behaviour. *Dalton Trans.* **2012**, *41*, 3248−3252.

(35) Das, S.; Dey, A.; Biswas, S.; Colacio, E.; Chandrasekhar, V. Hydroxide-free cubane-shaped tetranuclear $[Ln_4]$ complexes. *Inorg. Chem.* **2014**, *53*, 3417−3426.

(36) Kumar, P.; Flores Gonzalez, J.; Sahu, P. P.; Ahmed, N.; Acharya, J.; Kumar, V.; Cador, O.; Pointillart, F.; Singh, S. K.; Chandrasekhar, V. Magnetocaloric effect and slow magnetic relaxation in peroxide-assisted tetranuclear lanthanide assemblies. *Inorg. Chem. Front* **2022**, *9*, 5072−5092.

(37) Jami, A. K.; Baskar, V.; Sanudo, E. C. New structural form of a tetranuclear lanthanide hydroxo cluster: Dy_4 analogue display slow magnetic relaxation. *Inorg. Chem.* **2013**, *52*, 2432−2438.

(38) Wang, W. M.; Hu, X. Y.; Yang, Y.; Zhao, J. Q.; Zhang, Y. X.; Kang, X. M.; Wu, Z. L. Modulation of magnetic relaxation behaviors via replacing coordinated solvents in a series of linear tetranuclear Dy_4 complexes. *New J. Chem.* **2020**, *44*, 8494−8502.

(39) Sun, W. B.; Han, B. L.; Lin, P. H.; Li, H. F.; Chen, P.; Tian, Y. M.; Murugesu, M.; Yan, P. F. Series of dinuclear and tetranuclear lanthanide clusters encapsulated by salen-type and β-diketionate ligands: single-molecule magnet and fluorescence properties. *Dalton Trans.* **2013**, *42*, 13397−13403.

(40) Xue, Y. S.; Qiao, H.; Zhao, X. Y.; Liu, S. Y.; Xu, M.; Bai, L.; Wang, W. M. Two rhombus-shaped tetranuclear gadolinium clusters showing magnetic refrigeration. *Polyhedron* **2018**, *147*, 126−130.

(41) Chandrasekhar, V.; Hossain, S.; Das, S.; Biswas, S.; Sutter, J. P. Rhombus-shaped tetranuclear $[Ln_4]$ complexes [Ln= Dy(III) and Ho(III)]: synthesis, structure, and SMM behavior. *Inorg. Chem.* **2013**, *52*, 6346−6353.

(42) Goura, J.; Walsh, J. P.; Tuna, F.; Chandrasekhar, V. Tetranuclear lanthanide (III) complexes in a seesaw geometry: synthesis, structure, and magnetism. *Inorg. Chem.* **2014**, *53*, 3385−3391.

(43) Yu, H.; Yang, J. X.; Han, J. Q.; Li, P. F.; Hou, Y. L.; Wang, W. M.; Fang, M. Tetranuclear lanthanide complexes showing magnetic refrigeration and single molecule magnet behavior. *New J. Chem.* **2019**, *43*, 8067−8074.

(44) Biswas, S.; Das, S.; Hossain, S.; Bar, A. K.; Sutter, J. P.; Chandrasekhar, V. Tetranuclear Lanthanide (III) Complexes Containing a Square-Grid Core: Synthesis, Structure, and Magnetism. *Eur. J. Inorg. Chem.* **2016**, *28*, 4683−4692.

(45) Chen, P. Y.; Wu, M. Z.; Li, T.; Shi, X. J.; Tian, L.; Liu, Z. Y. Lanthanide Tetranuclear Cage and Mononuclear Cocrystalline Nitronyl Nitroxide Complex with Single-Molecule-Magnet Behavior. *Inorg. Chem.* **2018**, *57*, 12466−12470.

(46) Luan, F.; Liu, T.; Yan, P.; Zou, X.; Li, Y.; Li, G. Single-molecule magnet of a tetranuclear dysprosium complex disturbed by a salen-type ligand and chloride counterions. *Inorg. Chem.* **2015**, *54*, 3485−3490.

(47) Wu, Y.; Morton, S.; Kong, X.; Nichol, G. S.; Zheng, Z. Hydrolytic synthesis and structural characterization of lanthanide-acetylacetonato/hydroxo cluster complexes−A systematic study. *Dalton Trans.* **2011**, *40*, 1041−1046.

(48) Koo, B. H.; Lim, K. S.; Ryu, D. W.; Lee, W. R.; Koh, E. K.; Hong, C. S. Synthesis, structures and magnetic characterizations of isostructural tetranuclear Ln 4 clusters (Ln= Dy, Ho, and Eu). *Dalton Trans.* **2013**, *42*, 7204−7209.

(49) Xue, S.; Guo, Y. N.; Zhao, L.; Zhang, P.; Tang, J. Unique Y-shaped lanthanide aggregates and single-molecule magnet behaviour for the Dy_4 analogue. *Dalton Trans.* **2014**, *43*, 1564−1570.

(50) Baskar, V.; Roesky, P. W. Synthesis and structural characterization of a series of tetranuclear lanthanide clusters. *Z. Anorg. Allg. Chem.* **2005**, *631*, 2782−2785.

(51) Li, X.; Liu, Y.; Chi, X. W.; Zhu, G. Z.; Gao, F. Synthesis, Structures, and Magnetic Properties of Zigzag Tetranuclear Lanthanide Complexes. *Z. Anorg. Allg. Chem.* **2020**, *646*, 1292−1296.

(52) Tian, H.; Guo, Y. N.; Zhao, L.; Tang, J.; Liu, Z. Hexanuclear dysprosium (III) compound incorporating vertex-and edge-sharing Dy_3 triangles exhibiting single-molecule-magnet behavior. *Inorg. Chem.* **2011**, *50*, 8688−8690.

(53) Sessoli, R.; Powell, A. K. Strategies towards single molecule magnets based on lanthanide ions. *Coord. Chem. Rev.* **2009**, *253*, 2328−2341.

(54) Hewitt, I. J.; Tang, J.; Madhu, N. T.; Anson, C. E.; Lan, Y.; Luzon, J.; Etienne, M.; Sessoli, R.; Powell, A. K. Coupling Dy_3 triangles enhances their slow magnetic relaxation. *Angew. Chem.* **2010**, *122*, 6496−6500.

(55) Chandrasekhar, V.; Hossain, S.; Das, S.; Biswas, S.; Sutter, J. P. Rhombus-shaped tetranuclear $[Ln_4]$ complexes [Ln= Dy (III) and Ho (III)]: synthesis, structure, and SMM behavior. *Inorg. Chem.* **2013**, *52*, 6346−6353.

(56) Guo, P. H.; Liu, J.; Wu, Z. H.; Yan, H.; Chen, Y. C.; Jia, J. H.; Tong, M. L. Single-molecule-magnet behavior in a [2× 2] grid Dy^{III}_4 cluster and a dysprosium-doped Y^{III}_4 cluster. *Inorg. Chem.* **2015**, *54*, 8087−8092.

(57) Dawe, L. N.; Shuvaev, K. V.; Thompson, L. K. Polytopic ligand directed self-assembly—polymetallic [n× n] grids versus non-grid oligomers. *Chem. Soc. Rev.* **2009**, *38*, 2334−2359.

(58) Milway, V. A.; Abedin, S. T.; Niel, V.; Kelly, T. L.; Dawe, L. N.; Dey, S. K.; Thompson, D. W.; Miller, D. O.; Alam, M. S.; Müller, P.; Thompson, L. K. Supramolecular 'flat'Mn_9 grid complexes—towards functional molecular platforms. *Dalton Trans.* **2006**, *23*, 2835−2851.

(59) Dawe, L. N.; Shuvaev, K. V.; Thompson, L. K. Magnetic [n× n](n= 2− 5) grids by directed self-assembly. *Inorg. Chem.* **2009**, *48*, 3323−3341.

(60) Anwar, M. U.; Thompson, L. K.; Dawe, L. N.; Habib, F.; Murugesu, M. Predictable self-assembled [2× 2] Ln (III) $_4$ square grids (Ln= Dy, Tb)—SMM behaviour in a new lanthanide cluster motif. *Chem. Commun.* **2012**, *48*, 4576−4578.

(61) Yang, Q.; Ungur, L.; Wernsdorfer, W.; Tang, J. Toroidal magnetic moments in Tb 4 squares. *Inorg. Chem. Front.* **2022**, *9*, 784−791.

(62) Randell, N. M.; Anwar, M. U.; Drover, M. W.; Dawe, L. N.; Thompson, L. K. Self-assembled Ln (III) $_4$ (Ln= Eu, Gd, Dy, Ho, Yb) [2× 2] square grids: a new class of lanthanide cluster. *Inorg. Chem.* **2013**, *52*, 6731−6742.

(63) Woodruff, D. N.; Tuna, F.; Bodensteiner, M.; Winpenny, R. E.; Layfield, R. A. Single-molecule magnetism in tetrametallic terbium and dysprosium thiolate cages. *Organometallics* **2013**, *32*, 1224−1229.

(64) Xu, C.; Wu, Z.; Fan, C.; Yan, L.; Wang, W.; Ji, B. Synthesis of two lanthanide clusters LnIII4 (Gd_4 and Dy_4) with [2 × 2] square grid shape: Magnetocaloric effect and slow magnetic relaxation behaviors. *J. Rare Earths* **2021**, *39*, 1082−1088.

(65) Wu, S. Q.; Xie, Q. W.; An, G. Y.; Chen, X.; Liu, C. M.; Cui, A. L.; Kou, H. Z. Supramolecular lanthanide metallogrids exhibiting field-induced single-ion magnetic behavior. *Dalton Trans.* **2013**, *42*, 4369−4372.

(66) Ashebr, T. G.; Li, X. L.; Zhao, C.; Yang, Q.; Tang, J. Bis-pyrazolone-based dysprosium (III) complexes: zero-field single-molecule magnet behavior in the [2 × 2] grid $Dy(III)_4$ cluster. *CrystEngComm.* **2022**, *24*, 6688−6695.

(67) Huang, W.; Shen, F. X.; Wu, S. Q.; Liu, L.; Wu, D.; Zheng, Z.; Xu, J.; Zhang, M.; Huang, X. C.; Jiang, J.; Pan, F.; Li, Y.; Zhu, K.; Sato, O. Metallogrid single-molecule magnet: solvent-induced nuclearity transformation and magnetic hysteresis at 16 K. *Inorg. Chem.* **2016**, *55*, 5476−5484.

(68) Wu, J.; Lin, S. Y.; Shen, S.; Li, X. L.; Zhao, L.; Zhang, L.; Tang, J. Probing the magnetic relaxation and magnetic moment arrangement in a series of Dy_4 squares. *Dalton Trans.* **2017**, *46*, 1577−1584.

(69) Bi, Y.; Wang, X. T.; Liao, W.; Wang, X.; Deng, R.; Zhang, H.; Gao, S. Thiacalix [4] arene-Supported planar Ln_4 (Ln= Tb^{III}, Dy^{III}) clusters: toward luminescent and magnetic bifunctional materials. *Inorg. Chem.* **2009**, *48*, 11743−11747.

(70) Biswas, S.; Goura, J.; Das, S.; Topping, C. V.; Brambleby, J.; Goddard, P. A.; Chandrasekhar, V. Octanuclear heterobimetallic $\{Ni_4Ln_4\}$ assemblies possessing Ln_4 square grid [2 × 2] motifs:

synthesis, structure, and magnetism. *Inorg. Chem.* **2016**, *55*, 8422−8436.

(71) Wang, W. M.; Li, X. Z.; Zhang, L.; Chen, J. L.; Wang, J. H.; Wu, Z. L.; Cui, J. Z. A series of [2 × 2] square grid Ln^{III}_4 clusters: a large magnetocaloric effect and single-molecule-magnet behavior. *New J. Chem.* **2019**, *43*, 7419−7426.

(72) Xue, S.; Zhao, L.; Guo, Y. N.; Tang, J. A novel windmill-type Dy(III) [2 × 2] grid exhibiting slow magnetic relaxation. *Dalton Trans.* **2012**, *41*, 351−353.

(73) Gusev, A.; Herchel, R.; Nemec, I.; Shul'gin, V.; Eremenko, I. L.; Lyssenko, K.; Linert, W.; Trávníček, Z. Tetranuclear lanthanide complexes containing a hydrazone-type ligand. Dysprosium [2 × 2] gridlike single-molecule magnet and toroic. *Inorg. Chem.* **2016**, *55*, 12470−12476.

(74) Xue, S.; Zhao, L.; Guo, Y. N.; Chen, X. H.; Tang, J. Field enhanced thermally activated mechanism in a square Dy_4 aggregate. *Chem. Commun.* **2012**, *48*, 7031−7033.

(75) Das, C.; Vaidya, S.; Gupta, T.; Frost, J. M.; Righi, M.; Brechin, E. K.; Affronte, M.; Rajaraman, G.; Shanmugam, M. Single-Molecule Magnetism, Enhanced Magnetocaloric Effect, and Toroidal Magnetic Moments in a Family of Ln_4 Squares. *Chem. Eur. J.* **2015**, *21*, 15639−15650.

(76) Biswas, S.; Das, S.; van Leusen, J.; Kögerler, P.; Chandrasekhar, V. Tetranuclear [2 × 2] Square-Grid Lanthanide(III) Complexes: Syntheses, Structures, and Magnetic Properties. *Eur. J. Inorg. Chem.* **2014**, *25*, 4159−4167.

(77) Long, B. F.; Yu, S.; Zhu, Z. H.; Li, Y. L.; Liang, F. P.; Zou, H. H. Coordination site manipulation of the annular growth mechanism to assemble chiral lanthanide clusters with different shapes and magnetic properties. *Inorg. Chem. Front.* **2022**, *9*, 5950−5959.

(78) Biswas, S.; Das, S.; Hossain, S.; Bar, A. K.; Sutter, J. P.; Chandrasekhar, V. Tetranuclear Lanthanide(III) Complexes Containing a Square-Grid Core: Synthesis, Structure, and Magnetism. *Eur. J. Inorg. Chem.* **2016**, *28*, 4683−4692.

(79) (a) Soncini, A.; Chibotaru, L. F. Toroidal magnetic states in molecular wheels: Interplay between isotropic exchange interactions and local magnetic anisotropy. *Phys. Rev. B* **2008**, *77*, No. 220406. (b) Chibotaru, L.; Ungur, L.; Soncini, A. The origin of nonmagnetic Kramers doublets in the ground state of dysprosium triangles: evidence for a toroidal magnetic moment. *Angew. Chem.Int. Ed.* **2008**, *47*, 4126−4129.

(80) Luzon, J.; Bernot, K.; Hewitt, I. J.; Anson, C. E.; Powell, A. K.; Sessoli, R. Spin chirality in a molecular dysprosium triangle: the archetype of the noncollinear Ising model. *Phys. Rev. Lett.* **2008**, *100*, No. 247205.

(81) Fiebig, M. Revival of the magnetoelectric effect. *J. Phys. D. Appl. Phys.* **2005**, *38*, R123.

(82) Li, X. L.; Tang, J. Recent developments in single-molecule toroics. *Dalton Trans.* **2019**, *48*, 15358−15370.

(83) Ungur, L.; Lin, S. Y.; Tang, J.; Chibotaru, L. F. Single-molecule toroics in Ising-type lanthanide molecular clusters. *Chem. Soc. Rev.* **2014**, *43*, 6894−6905.

(84) Guo, P. H.; Liu, J. L.; Zhang, Z. M.; Ungur, L.; Chibotaru, L. F.; Leng, J. D.; Guo, F. S.; Tong, M. L. The first {Dy_4} single-molecule magnet with a toroidal magnetic moment in the ground state. *Inorg. Chem.* **2012**, *51*, 1233−1235.

(85) Gysler, M.; El Hallak, F.; Ungur, L.; Marx, R.; Hakl, M.; Neugebauer, P.; Rechkemmer, Y.; Lan, Y.; Sheikin, I.; Orlita, M.; Anson, C. E.; et al. Multitechnique investigation of Dy_3−implications for coupled lanthanide clusters. *Chem. Sci.* **2016**, *7*, 4347−4354.

(86) Luzon, J.; Bernot, K.; Hewitt, I. J.; Anson, C. E.; Powell, A. K.; Sessoli, R. Spin chirality in a molecular dysprosium triangle: the archetype of the noncollinear Ising model. *Phys. Rev. Lett.* **2008**, *100*, 1−4.

(87) Novitchi, G.; Pilet, G.; Ungur, L.; Moshchalkov, V. V.; Wernsdorfer, W.; Chibotaru, L. F.; Luneau, D.; Powell, A. K. Heterometallic Cu^{II}/Dy^{III} 1D chiral polymers: chirogenesis and exchange coupling of toroidal moments in trinuclear Dy_3 single molecule magnets. *Chem. Sci.* **2012**, *3*, 1169−1176.

(88) Zhong, L.; Chen, W. B.; OuYang, Z. J.; Yang, M.; Zhang, Y. Q.; Gao, S.; Schulze, M.; Wernsdorfer, W.; Dong, W. Unprecedented one-dimensional chain and two-dimensional network dysprosium(III) single-molecule toroics with white-light emission. *Chem. Commun.* **2020**, *56*, 2590−2593.

(89) Xue, S.; Chen, X. H.; Zhao, L.; Guo, Y. N.; Tang, J. Two bulky-decorated triangular dysprosium aggregates conserving vortex-spin structure. *Inorg. Chem.* **2012**, *51*, 13264−13270.

(90) Wang, Y. X.; Shi, W.; Li, H.; Song, Y.; Fang, L.; Lan, Y.; Powell, A. K.; Wernsdorfer, W.; Ungur, L.; Chibotaru, L. F.; Shen, M.; Cheng, P. A single-molecule magnet assembly exhibiting a dielectric transition at 470 K. *Chem. Sci.* **2012**, *3*, 3366−3370.

(91) Li, X. L.; Wu, J.; Tang, J.; Le Guennic, B.; Shi, W.; Cheng, P. A planar triangular Dy^{3+} Dy_3 single-molecule magnet with a toroidal magnetic moment. *Chem. Commun.* **2016**, *52*, 9570−9573.

(92) Lin, S. Y.; Wernsdorfer, W.; Ungur, L.; Powell, A. K.; Guo, Y. N.; Tang, J.; Zhao, L.; Chibotaru, L. F.; Zhang, H. J. Coupling Dy_3 triangles to maximize the toroidal moment. *Angew. Chem., Int. Ed.* **2012**, *51*, 12767−12771.

(93) Baniodeh, A.; Magnani, N.; Bräse, S.; Anson, C. E.; Powell, A. K. Ligand field variations: tuning the toroidal moment of Dy_6 rings. *Dalton Trans.* **2015**, *44*, 6343−6347.

(94) Wu, J.; Cador, O.; Li, X. L.; Zhao, L.; Le Guennic, B.; Tang, J. Axial ligand field in D_{4d} coordination symmetry: Magnetic relaxation of Dy SMMs perturbed by counteranions. *Inorg. Chem.* **2017**, *56*, 11211−11219.

(95) Ungur, L.; Langley, S. K.; Hooper, T. N.; Moubaraki, B.; Brechin, E. K.; Murray, K. S.; Chibotaru, L. F. Net toroidal magnetic moment in the ground state of a {Dy_6}-triethanolamine ring. *J. Am. Chem. Soc.* **2012**, *134*, 18554−18557.

(96) Langley, S. K.; Moubaraki, B.; Forsyth, C. M.; Gass, I. A.; Murray, K. S. Structure and magnetism of new lanthanide 6-wheel compounds utilizing triethanolamine as a stabilizing ligand. *Dalton Trans.* **2010**, *39*, 1705−1708.

(97) Wu, J.; Li, X. L.; Guo, M.; Zhao, L.; Zhang, Y. Q.; Tang, J. Realization of toroidal magnetic moments in heterometallic 3d−4f metallocycles. *Chem. Commun.* **2018**, *54*, 1065−1068.

(98) Wu, J.; Zhao, L.; Zhang, L.; Li, X. L.; Guo, M.; Powell, A. K.; Tang, J. Macroscopic Hexagonal Tubes of 3d−4f Metallocycles. *Angew. Chem.* **2016**, *128*, 15803−15807.

(99) Fernandez Garcia, G.; Guettas, D.; Montigaud, V.; Larini, P.; Sessoli, R.; Totti, F.; Cador, O.; Pilet, G.; Le Guennic, B. A Dy_4 Cubane: A New Member in the Single-Molecule Toroics Family. *Angew. Chem.* **2018**, *130*, 17335−17339.

(100) Vignesh, K. R.; Rajaraman, G. Strategies to design single-molecule toroics using triangular {Ln3} n motifs. *ACS omega* **2021**, *6* (48), 32349−32364.

(101) Chauhan, D.; Vignesh, K. R.; Swain, A.; Langley, S. K.; Murray, K. S.; Shanmugam, M.; Rajaraman, G. Exploiting Strong {CrIII−DyIII} Ferromagnetic Exchange Coupling to Quench Quantum Tunneling of Magnetization in a Novel {CrIII2DyIII3} Single-Molecule Magnet. *Cryst. Growth Des.* **2023**, *23*, 197−206.

(102) Caporale, C.; Sobolev, A. N.; Phonsri, W.; Murray, K. S.; Swain, A.; Rajaraman, G.; Ogden, M. I.; Massi, M.; Fuller, R. O. Lanthanoid pyridyl-β-diketonate 'triangles'. New examples of single molecule toroics. *Dalton Trans.* **2020**, *49*, 17421−17432.

(103) Kaboudin, B.; Haghighat, H.; Yokomatsu, T. A novel method for the separation of bis (α-hydroxyalkyl) phosphinic acid diastereoisomers via formation of novel cyclic phosphinic acids. *J. Org. Chem.* **2006**, *71*, 6604−6606.

(104) Kaboudin, B.; As-habei, N. A novel synthesis of bis-(α-hydroxyalkyl) phosphinic acids involving microwave irradiation. *Tetrahedron Lett.* **2004**, *45*, 9099−9101.

(105) (a) Tian, H.; Zhao, L.; Tang, J. Exploiting Miraculous atmospheric CO_2 fixation in the design of dysprosium single-molecule magnets. *Cryst. Growth Des.* **2018**, *18*, 1173−1181. (b) Kim, P.; Anderko, A.; Navrotsky, A.; Riman, R. E. Trends in structure and thermodynamic properties of normal rare earth carbonates and rare earth hydroxycarbonates. *Minerals* **2018**, *8*, 106. (c) Kalatha, S.;

Perraki, M.; Economou-Eliopoulos, M.; Mitsis, I. On the Origin of Bastnaesite-(La,Nd,Y) in the Nissi (Patitira) Bauxite Laterite Deposit, Lokris, Greece. *Minerals* **2017**, *7*, 45.

(106) Benelli, C.; Gatteschi, D. *Introduction to Molecular Magnetism: From Transition Metals to Lanthanides*; John Wiley & Sons, 2015.

(107) Dekker, C.; Arts, A. F. M.; De Wijn, H. W.; Van Duyneveldt, A. J.; Mydosh, J. A. Activated dynamics in a two-dimensional Ising spin glass: $Rb_2Cu_{1-x}Co_xF_4$. *Phys. Rev. B* **1989**, *40*, 11243.

(108) Cole, K. S.; Cole, R. H. Dispersion and absorption in dielectrics I. Alternating current characteristics. *J. Chem. Phys.* **1941**, *9*, 341−351.

(109) Guo, F. S.; Day, B. M.; Chen, Y. C.; Tong, M. L.; Mansikkamäki, A.; Layfield, R. A. Magnetic hysteresis up to 80 K in a dysprosium metallocene single-molecule magnet. *Science* **2018**, *362*, 1400−1403.

(110) Randall McClain, K.; Gould, C. A.; Chakarawet, K.; Teat, S. J.; Groshens, T. J.; Long, J. R.; Harvey, B. G. High-temperature magnetic blocking and magneto-structural correlations in a series of dysprosium(III) metallocenium single-molecule magnets. *Chem. Sci.* **2018**, *9*, 8492−8503.

(111) Goodwin, C. A.; Ortu, F.; Reta, D.; Chilton, N. F.; Mills, D. P. Molecular magnetic hysteresis at 60 K in dysprosocenium. *Nature* **2017**, *548*, 439−442.

(112) Vincent, A. H.; Whyatt, Y. L.; Chilton, N. F.; Long, J. R. Strong Axiality in a dysprosium (III) bis (borolide) complex leads to magnetic blocking at 65 K. *J. Am. Chem. Soc.* **2023**, *145*, 1572−1579.

(113) Caporale, C.; Sobolev, A. N.; Phonsri, W.; Murray, K. S.; Swain, A.; Rajaraman, G.; Ogden, M. I.; Massi, M.; Fuller, R. O. Lanthanoid pyridyl-β-diketonate 'triangles'. New examples of single molecule toroics. *Dalton Trans.* **2020**, *49*, 17421−17432.

(114) Lines, M. Orbital angular momentum in the theory of paramagnetic clusters. *J. Chem. Phys.* **1971**, *55*, 2977−2984.

(115) Vignesh, K. R.; Langley, S. K.; Swain, A.; Moubaraki, B.; Damjanović, M.; Wernsdorfer, W.; Rajaraman, G.; Murray, K. S. Slow Magnetic Relaxation and Single-Molecule Toroidal Behaviour in a Family of Heptanuclear {CrIIILnIII6}(Ln= Tb, Ho, Er) Complexes. *Angew. Chem.* **2018**, *130*, 787−792.

(116) (a) Leng, J. D.; Liu, J. L.; Lin, W. Q.; Gómez-Coca, S.; Aravena, D.; Ruiz, E.; Tong, M. L. Unprecedented ferromagnetic dipolar interaction in a dinuclear holmium (III) complex: a combined experimental and theoretical study. *Chem. Commun.* **2013**, *49*, 9341−9343. (b) Hymas, K.; Soncini, A. The Role of Magnetic Dipole—Dipole Coupling in Quantum Single-Molecule Toroics. *Magnetochemistry* **2022**, *8*, 58.

(117) Miller, J. S.; Drillon, M. *Magnetism: Molecules to Materials IV*; Wiley-VCH, 2002.

(118) Kumar, P.; Swain, A.; Acharya, J.; Li, Y.; Kumar, V.; Rajaraman, G.; Colacio, E.; Chandrasekhar, V. Synthesis, structure, and zero-field SMM behavior of homometallic Dy2, Dy4, and Dy6 complexes. *Inorg. Chem.* **2022**, *61*, 11600−11621.

(119) Langley, S. K.; Vignesh, K. R.; Moubaraki, B.; Rajaraman, G.; Murray, K. S. Oblate versus prolate electron density of lanthanide ions: A design criterion for engineering toroidal moments? A case study on {LnIII6}(Ln= Tb, Dy, Ho and Er) wheels. *Chem. Eur. J.* **2019**, *25*, 4156−4165.

(120) (a) Spaldin, N. A.; Fiebig, M.; Mostovoy, M. The toroidal moment in condensed-matter physics and its relation to the magnetoelectric effect. *J. Condens. Matter Phys.* **2008**, *20*, No. 434203. (b) Langley, S. K.; Vignesh, K. R.; Gupta, T.; Gartshore, C. J.; Rajaraman, G.; Forsyth, C. M.; Murray, K. S. New examples of triangular terbium (III) and holmium (III) and hexagonal dysprosium (III) single molecule toroics. *Dalton Trans.* **2019**, *48*, 15657−15667.

(121) Dolomanov, O. V.; Bourhis, L. J.; Gildea, R. J.; Howard, J. A. K.; Puschmann, H. OLEX2: a complete structure solution, refinement and analysis program. *J. Appl. Crystallogr.* **2009**, *42*, 339−341.

(122) Sheldrick, G. M. SHELXT−Integrated space-group and crystal-structure determination. *Acta Crystallogr. A* **2015**, *71*, 3−8.

(123) Sheldrick, G. M. Crystal structure refinement with SHELXL. *Acta Crystallogr. C Struct. Chem.* **2015**, *71*, 3−8.

(124) Bourhis, L. J.; Dolomanov, O. V.; Gildea, R. J.; Howard, J. A.; Puschmann, H. The anatomy of a comprehensive constrained, restrained refinement program for the modern computing environment−Olex2 dissected. *Acta Crystallogr. A: Found. Adv.* **2015**, *71*, 59−75.